Tsunami Hazard Maps of the Chehalis, Hoquiam, Willapa, and Wishkah Rivers—Model Results from a L1 Mw 9.0 Cascadia Subduction Zone Megathrust Earthquake Scenario

Grays Harbor and Pacific Counties

Alexander Dolcimascolo, Daniel W. Eungard, and Corina Allen

WASHINGTON STATE DEPT OF NATURAL RESOURCES
WASHINGTON GEOLOGICAL SURVEY

N
4 miles
MAP SCALE 1:48,000 (Maps 1–3)

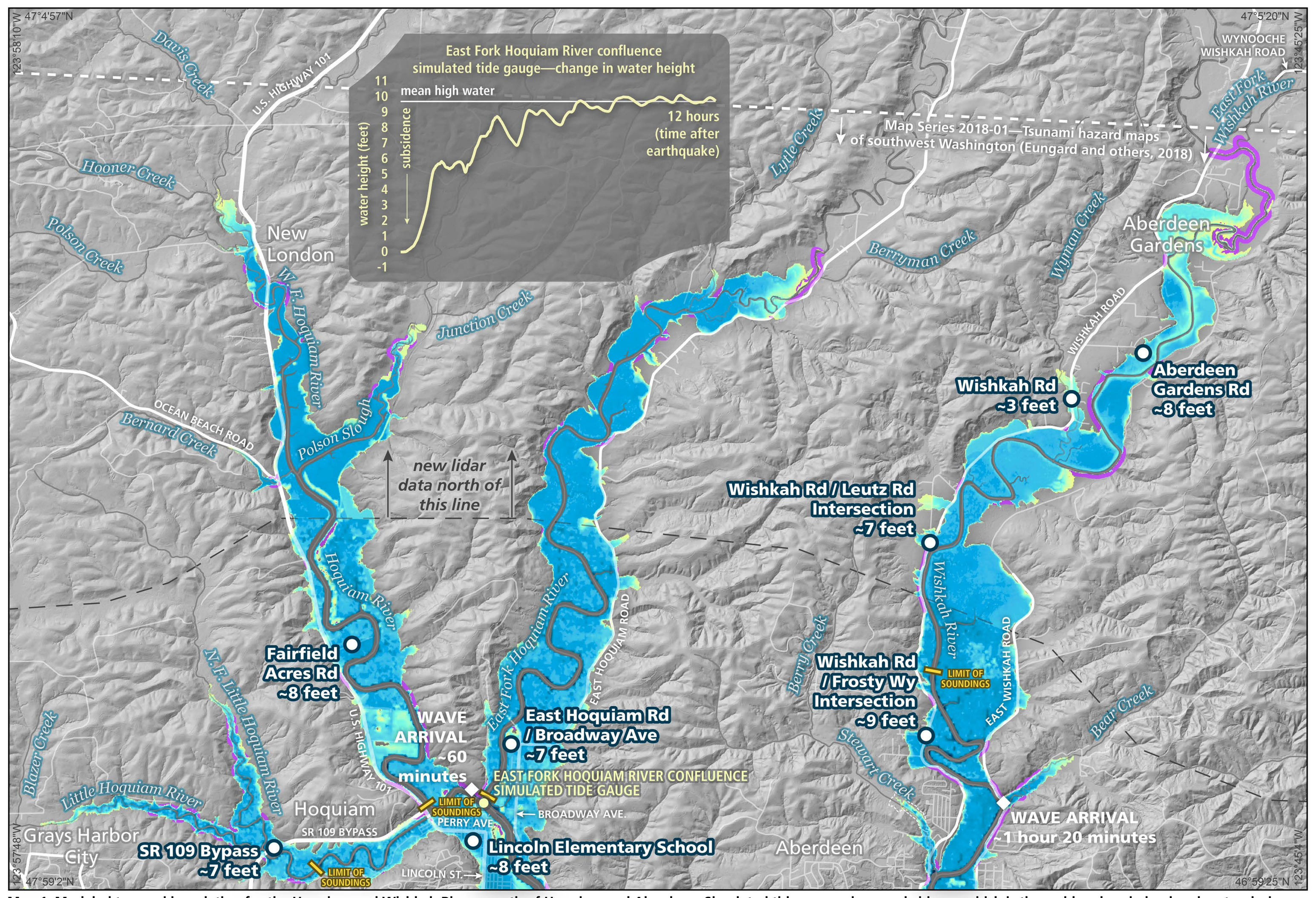

Map 1. Modeled tsunami inundation for the Hoquiam and Wishkah Rivers, north of Hoquiam and Aberdeen. Simulated tide gauge shows subsidence which is the sudden drop in land and water during earthquake shaking.

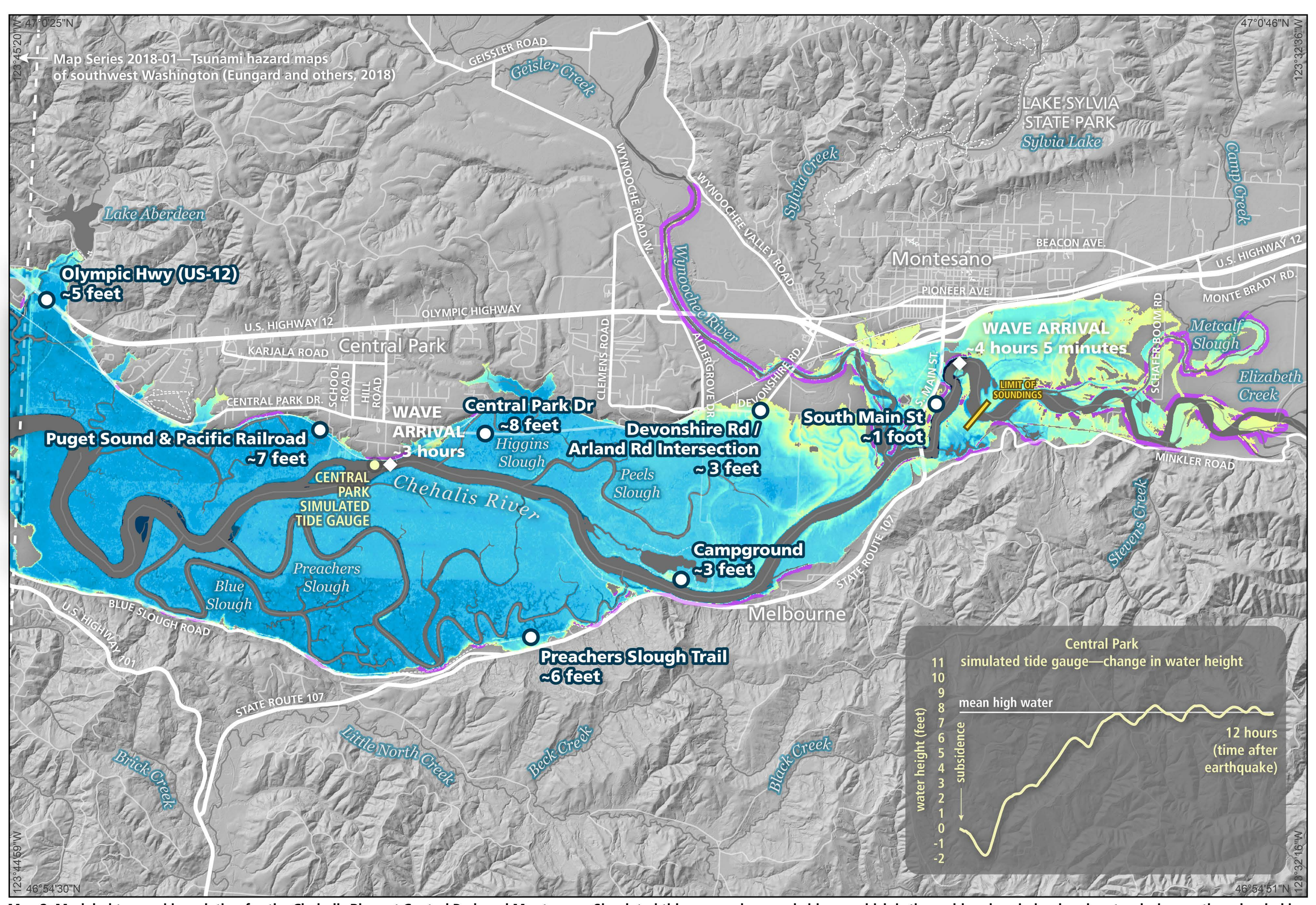

Map 2. Modeled tsunami inundation for the Chehalis River at Central Park and Montesano. Simulated tide gauge shows subsidence which is the sudden drop in land and water during earthquake shaking.

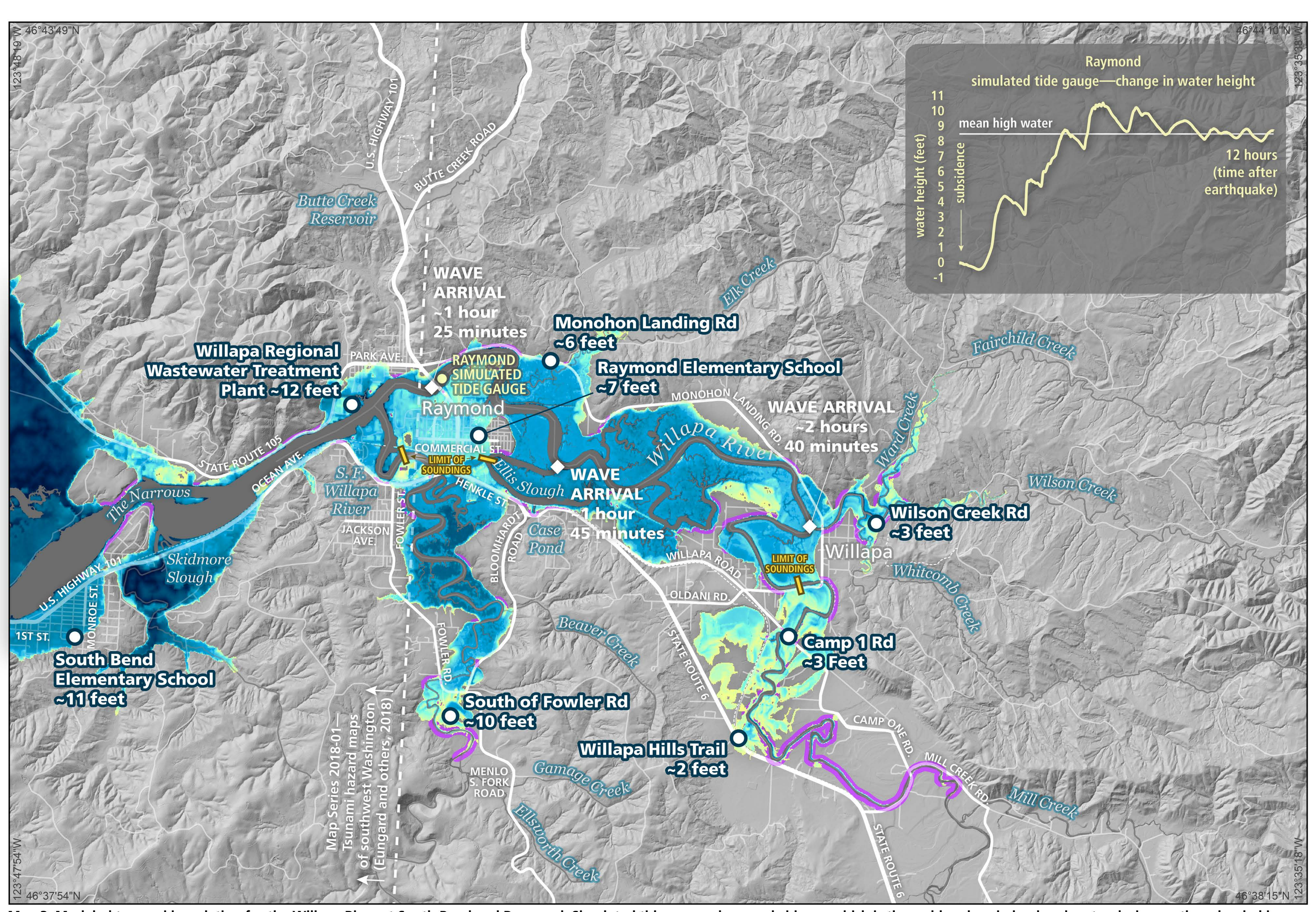

Map 3. Modeled tsunami inundation for the Willapa River at South Bend and Raymond. Simulated tide gauge shows subsidence which is the sudden drop in land and water during earthquake shaking.

Figure 1

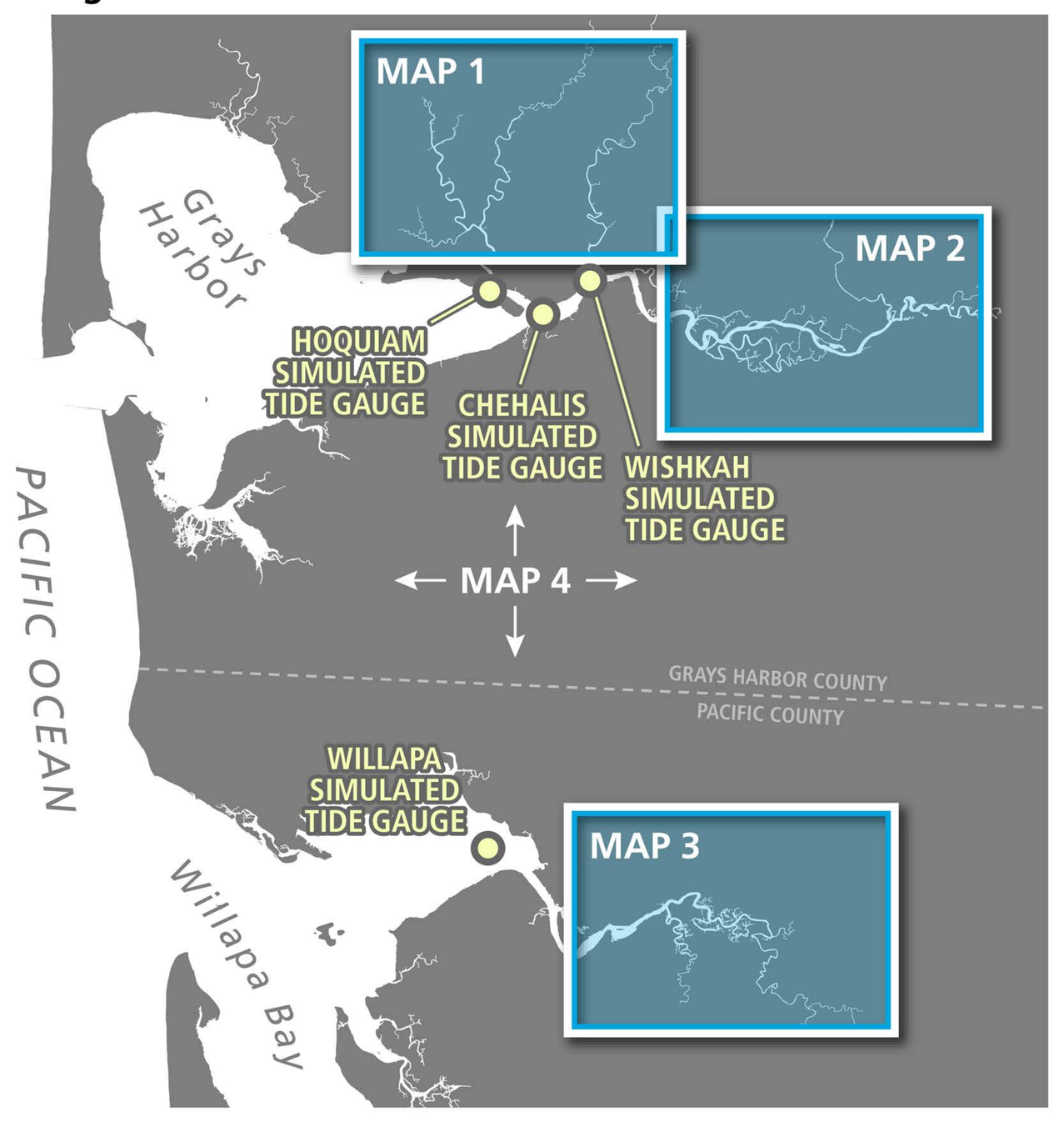

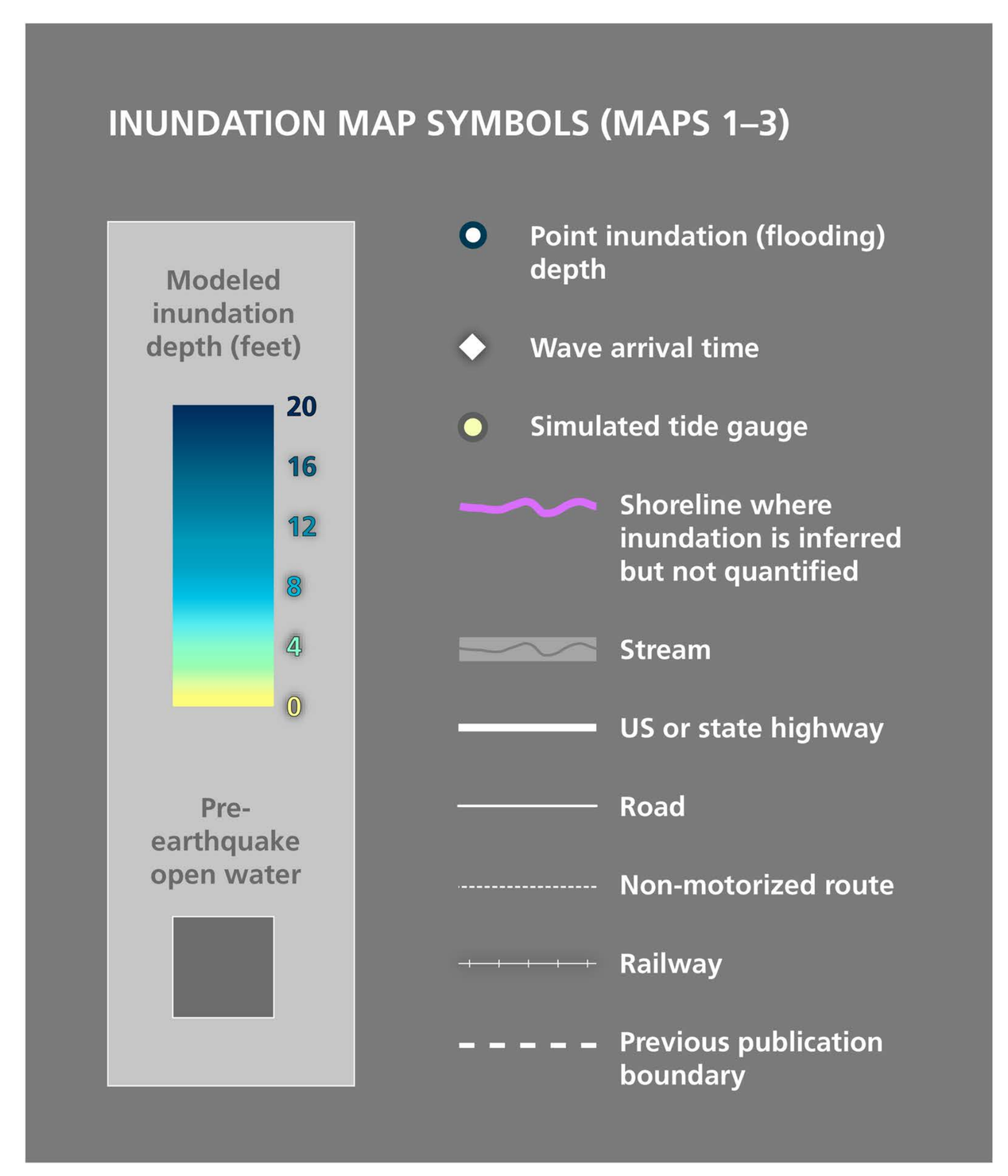

ABSTRACT

We present results from new tsunami inundation and current-speed modeling for a magnitude 9.0 Cascadia subduction zone earthquake scenario for the Chehalis, Hoquiam, Willapa, and Wishkah Rivers in southwest Washington. This tsunami modeling is a continuation of previous modeling published in 2018 by the Washington Geological Survey for areas surrounding Willapa Bay and Grays Harbor. That modeling needed to be expanded as it did not cover upriver areas. This new study uses the same earthquake scenario as the 2018 publication, with an updated Digital Elevation Model (DEM) to better understand how far up rivers the tsunami inundation would reach. The seismic scenario used here generates subsidence that will affect all coastal elevations in this study area as a result of earthquake-induced land deformation. The impact of subsidence on the first tsunami-driven wave arrival is significant in this study area, as it generally masks the leading trough-phase of the tsunami observed in other parts of the Washington coastline (such as the Salish Sea). The initial tsunami arrives quickly—within 20 minutes at all river mouths modeled in this study area, leaving limited time for official tsunami alerts. Maximum changes in tsunami water heights following the earthquake exceed ~10 feet (~3 meters) at all river mouths, with the highest height of ~15 feet (~4.5 meters) impacting the Willapa River. The tsunami also travels a minimum of ~8 river miles (13 kilometers) upriver in all four river valleys. The farthest modeled upriver flooding extent is up the Chehalis River, where the tsunami travels ~13 miles (21 kilometers) upriver. Although the majority of tsunami inundation in this study area is confined to mapped floodplains, inundation impacting roadways may isolate communities upriver. This study is limited in that modeling does not account for variable tide stage, tidal currents, riverine flow, earthquake-induced landslides, seiches, liquefaction, or minor topographic changes that would locally modify the effects of tsunami waves. In addition, there are many assumptions associated with the scenario earthquake modeled here. Due to these limitations, this modeling may not be suitable for site-specific tsunami inundation assessment or for determining effects on the built environment. This modeling can be used as a tool to assist with emergency preparations and evacuation planning prior to a Cascadia subduction zone event or to determine locations where a tsunami vertical evacuation refuge may be appropriate.

INTRODUCTION

The Cascadia subduction zone (CSZ) stretches for about 775 miles (1,250 kilometers) along the Pacific Ocean from Cape Mendocino, California to just north of Vancouver Island, Canada. The CSZ is the interface where the Juan de Fuca, Explorer, and Gorda oceanic plates slide beneath the North American continental plate. This subduction process periodically generates great earthquakes when built up strain abruptly releases. These earthquakes can produce tsunamis that pose a significant hazard to Washington and possibly to other coastlines along the Pacific Ocean. Research over the last few decades illustrates the impacts of CSZ earthquakes and tsunamis along the shorelines of British Columbia (Hutchinson and Clague, 2017), Washington (Atwater, 1992; Atwater and others, 1995), Oregon (Kelsey and others, 2005), and northern California (Padgett and others, 2021). Physical evidence demonstrates that these events have happened many times in the geologic record, with an average recurrence of every 220 to 540 years, and the most recent event taking place in the year 1700 (Atwater and Hemphill-Haley, 1997; Witter and others, 2011; Goldfinger and others, 2012).

A key component of tsunami hazard assessment, and the first step in developing evacuation plans, is to identify areas subject to tsunami inundation (flooding caused by tsunami waves). This study focuses on modeling maximum tsunami inundation and current speeds along river valleys in southwest Washington from the Cascadia L1 earthquake scenario (Witter and others, 2011). This tsunamigenic earthquake scenario is estimated to encompass 95 percent of the maximum inundation modeled in a suite of hypothetical CSZ tsunami scenarios (Witter and others, 2011) and closely approximates a ~2,500-year recurrence event, which is unlikely to be exceeded in the next CSZ earthquake. Results presented here specifically expand on the previous tsunami inundation modeling for the surrounding areas of Grays Harbor and Willapa Bay from Eungard and others (2018) by simulating the continuation of tsunami propagation along the Chehalis, Hoquiam, Willapa, and Wishkah Rivers. In comparison to the earlier publication, the map sheet and discussion presented here does not provide as detailed a review of the earthquake source, modeling methods, and modeling assumptions. To read more about these components of the modeling, we refer you to Eungard and others (2018).

METHODS AND MODELING

The digital elevation model (DEM) data used in the existing tsunami inundation modeling in southwest Washington (Eungard and others, 2018) were incomplete and did not extend up major river valleys. As a result, inundation for these important areas could not be modeled. In this publication, we incorporated new lidar data (USGS, 2019a,b) for previously missing areas of the DEM (NOAA NGDC, 2012) to produce new tsunami inundation maps for southwest Washington rivers. To better characterize each river, we also incorporated river depth measurements (soundings) published in NOAA hydrographic surveys and nautical charts (Office of Coast Survey, 2023) where available. These datasets were converted to Mean High Water (MHW) and then merged into the DEM to complete tsunami modeling. Upstream of the soundings, where no depth measurements are available, the river elevations are hydroflattened.

The tsunami modeling results presented in this study use the GeoClaw numerical modeling software package, an open-source code (part of the Clawpack software) that was initiated at the University of Washington (UW) and is still being developed by the UW tsunami modeling group in collaboration with other contributors (Clawpack Development Team, 2023). GeoClaw solves the nonlinear shallow water equations that simulate tsunami generation, propagation, and inundation given specific earthquake and bathymetry inputs. This is executed through using a finite volume method and an adaptive mesh refinement (AMR) strategy to calculate water surface elevations and velocities on a fine grid covering the region of interest and record the maximum values over the full simulation time (George, 2006, 2008; George and LeVeque, 2006; Berger and others, 2011; LeVeque and others, 2011; Mandli and others, 2016).

The modeling for the 2018 publication that this map builds on was developed using the Method of Splitting Tsunami (MOST) software package (Eungard and others, 2018; refer to previous publication for details and documentation about the MOST software). Both GeoClaw and the previously used MOST model have been validated through benchmark tests and are approved by the National Tsunami Hazard Mitigation Program (NTHMP) for use in developing tsunami inundation models (Synolakis and others, 2007; González and others, 2011; Horrillo and others, 2015). To test the practical equivalence between the two software packages, comparative simulations were performed for Bainbridge Island, WA (Titov and others, 2018), which produced close agreement between model results.

RESULTS

Maps and figures on this map sheet provide model results showing tsunami inundation distances, maximum onshore tsunami flooding depths, tsunami wave arrival times, and maximum current speeds using the CSZ L1 scenario for four main river valleys emptying into Grays Harbor and Willapa Bay. From north to south, these are the Hoquiam and Wishkah Rivers (Map 1), the Chehalis River (Map 2), and the Willapa River (Map 3). An overview of these three map areas is shown in Figure 1. An overview of tsunami current speeds for both Grays Harbor, Willapa Bay, and their surrounding river valleys is shown in Map 4.

Subsidence

All of the coastal areas included within this study are located close to the subduction zone, which means that land elevation drops during a modeled L1 earthquake scenario. This drop, known as subsidence, may cause local flooding prior to the onset of tsunami flooding that may impact the shoreline. It could also lead to a relative rise in sea level compared to the pre-earthquake shoreline once the tsunami event is over (Fig. 2). Coastal subsided lands falling below the high tide water level would effectively be lost land for potentially decades to centuries.

The modeled land surface deformation caused by the L1 scenario indicates that the most significant drop in elevations within this study area occur at the mouths of each river (where the rivers enter the bay), highlighted on Figure 2. Each river mouth subsides approximately 9–10 feet (~3 meters) in this model. This deformation pattern also indicates that subsidence values tend to decrease in both east and west directions from these locations, causing non-uniform, sloping subsidence over the region. Although this modeling did not include natural riverine flow or dynamic tides, it is possible that this subsidence pattern could also impact typical flow directions along the east–west flowing Chehalis and Willapa Rivers, depending on the tide stage at the time of the earthquake shaking. This all ensues while the temporary new sea level (which drops suddenly along with the land surface when the earthquake happens) also begins to dynamically recover back to the pre-earthquake level over a period of several hours (in our tsunami model, this level is the regional MHW datum). This recovery may also coalesce with the arrival of the first tsunami wave, potentially engulfing any initial trough phase (receding wave) of the tsunami, and instead amplify water heights.

In the tsunami model, synthetic tide gauges were placed at the mouths of the Chehalis, Hoquiam, Willapa, and Wishkah Rivers to record water level variations over the course of the simulated tsunami (Fig. 1). The tide gauges for the Chehalis, Hoquiam, and Willapa Rivers captured the recovery phenomenon described above as the initial trough phase of the tsunami arrival was absent (Figs. 3–5, respectively). The only river mouth to record any sign of falling water levels following the earthquake was the Wishkah River (Fig. 6), which is far enough east of the simulated earthquake rupture area to capture the leading tsunami trough phase expected in locations farther from the CSZ rupture, like Washington's inner waterways (Dolcimascolo and others, 2021). Other tide gauges placed farther upriver also record the leading trough of the simulated tsunami (see Map 2, Central Park gauge; and Map 3, Raymond gauge).

The modeled subsidence presented here is considered conservative in the sense that it uses values greater than the greatest known paleoseismic subsidence observation recorded on land in Washington, which is ~6 ft (1.76 m) near Cosmopolis (Atwater, 1988; Leonard and others, 2010). At this location, the L1 scenario returned a subsidence value that is greater than what was measured on land, between 8–9 feet (~2.5 meters). In a real earthquake event, actual subsidence values are dependent on the earthquake rupture geometry and are likely to be different from the L1 scenario presented here.

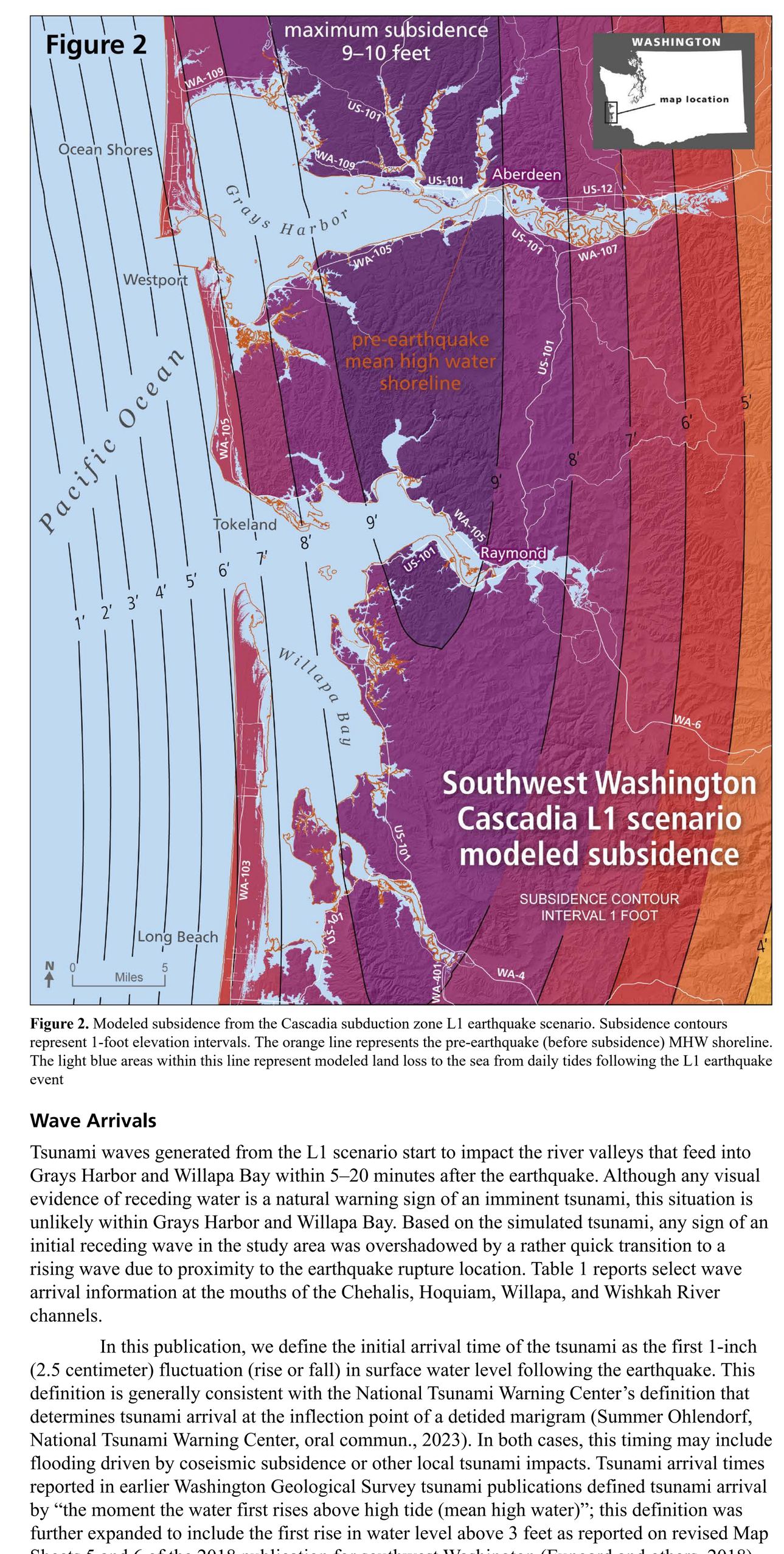

Figure 2. Modeled subsidence from the Cascadia subduction zone L1 earthquake scenario. Subsidence contours represent 1-foot elevation intervals. The orange line represents the pre-earthquake (before subsidence) MHW shoreline. The light blue areas within this line represent modeled land loss to the sea from daily tides following the L1 earthquake event

Wave Arrivals

Tsunami waves generated from the L1 scenario start to impact the river valleys that feed into Grays Harbor and Willapa Bay within 5–20 minutes after the earthquake. Although any visual evidence of receding water is a natural warning sign of an imminent tsunami, this situation is unlikely within Grays Harbor and Willapa Bay. Based on the simulated tsunami, any sign of an initial receding wave in the study area was overshadowed by a rather quick transition to a rising wave due to proximity to the earthquake rupture location. Table 1 reports select wave arrival information at the mouths of the Chehalis, Hoquiam, Willapa, and Wishkah River channels.

In this publication, we define the initial arrival time of the tsunami as the first 1-inch (2.5 centimeter) fluctuation (rise or fall) in surface water level following the earthquake. This definition is generally consistent with the National Tsunami Warning Center's definition that determines tsunami arrival at the inflection point of a detided marigram (Summer Ohlendorf, National Tsunami Warning Center, oral commun., 2023). In both cases, this timing may include flooding driven by coseismic subsidence or other local tsunami impacts. Tsunami arrival times reported in earlier Washington Geological Survey tsunami publications defined tsunami arrival by "the moment the water first rises above high tide (mean high water)"; this definition was further expanded to include the first rise in water level above 3 feet as reported on revised Map Sheets 5 and 6 of the 2018 publication for southwest Washington (Eungard and others, 2018). This expanded definition is reflected in Table 1 and Maps 1–3, where we report the 3-foot modeled wave arrival time. The 3-foot wave arrival times listed in this publication and in Eungard and others (2018) are similar, though not exactly the same due to differences in the tsunami model software used.

The arrival time of the highest water height recorded at each river mouth following the earthquake is listed in Table 1. Note that this timing does not represent the arrival of the largest wave; the largest wave is the one with the most dramatic change from the previous peak or trough. In all four modeled rivers, the first tsunami wave is the largest, yielding changes in water heights between 7 and 12 feet (~2 and ~3.5 meters) at the entrance of each river valley approximately 1–1.5 hours after the earthquake.

Table 1. Estimated time of tsunami wave arrival (rounded to 5-minute intervals). Initial arrival time represents a ±1 inch (2.5 centimeter) change in water height following the earthquake. The 3-foot wave arrival time is provided here for comparison with Map Sheets 5 and 6 of Eungard and others (2018). The highest water height arrival time is defined as the amount of time it takes for the water level to be at its highest recorded level for the entire tsunami simulation.

River mouth	Longitude (degrees)	Latitude (degrees)	Initial arrival time ± 1" (2.5 cm)(minutes)	3 foot wave arrival time (minutes)	Highest water height arrival time	Highest water height (feet)
Chehalis	-123.841587	46.957738	20 (rising wave)	60	6 hours, 40 minutes	10.5
Hoquiam	-123.878453	46.968969	5 (rising wave)	55	4 hours, 40 minutes	11.5
Willapa	-123.848283	46.708302	10 (rising wave)	45	4 hours, 40 minutes	15
Wishkah	-123.808557	46.973852	10 (falling wave)	65	5 hours	10.5

Figure 3. Chehalis simulated tide gauge

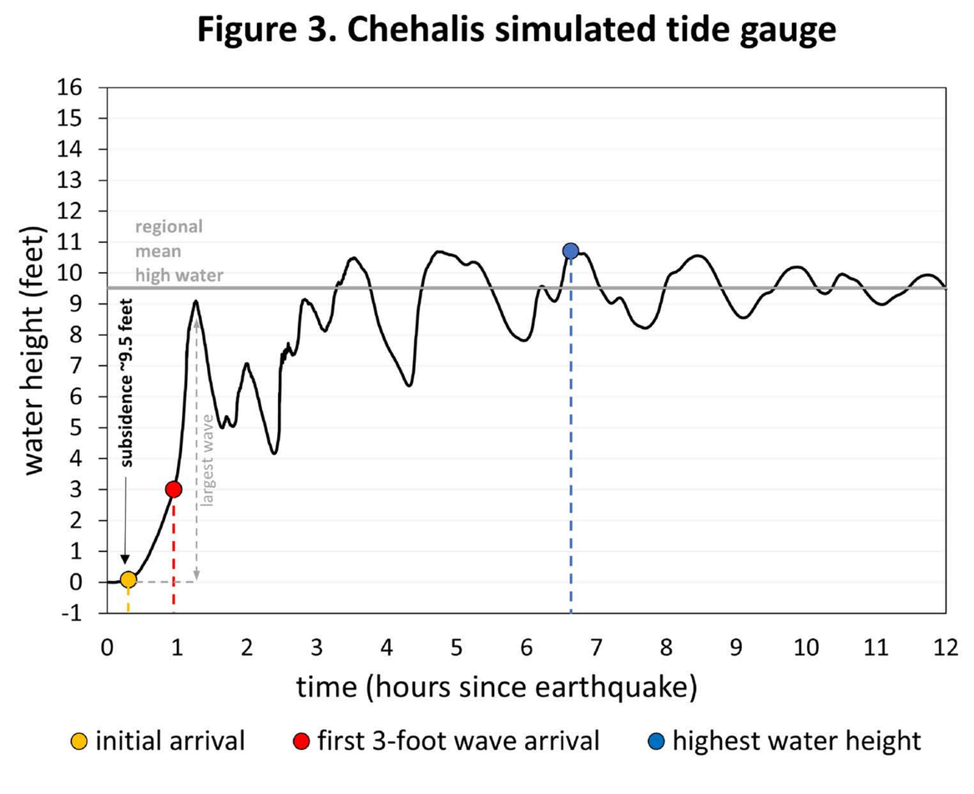

Figure 4. Hoquiam simulated tide gauge

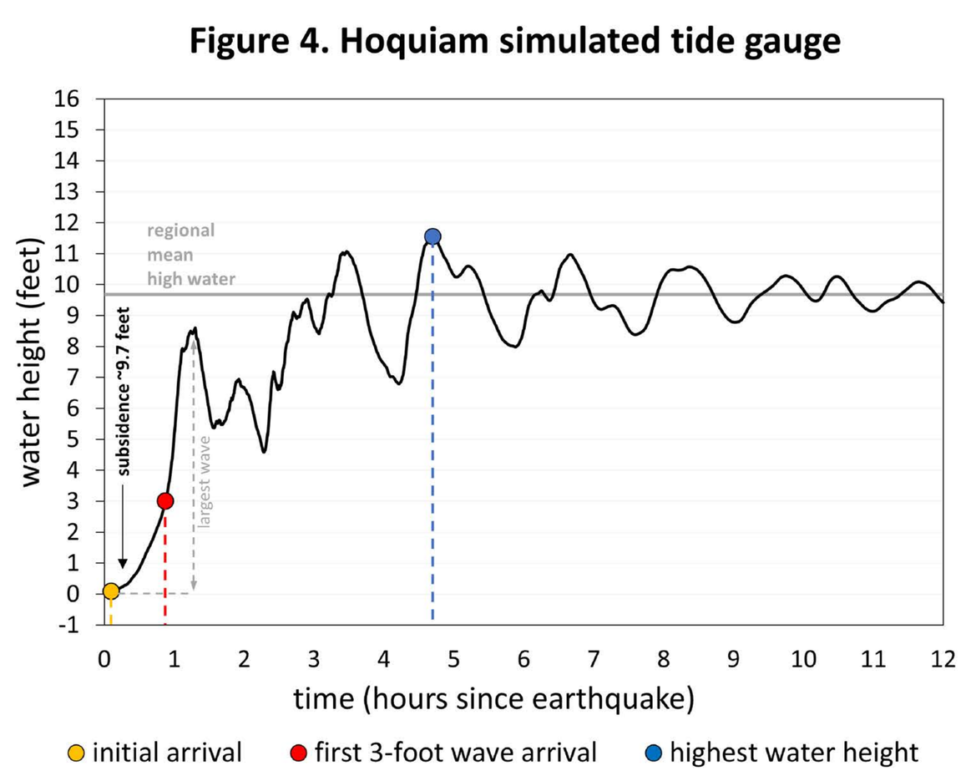

Figure 5. Willapa simulated tide gauge

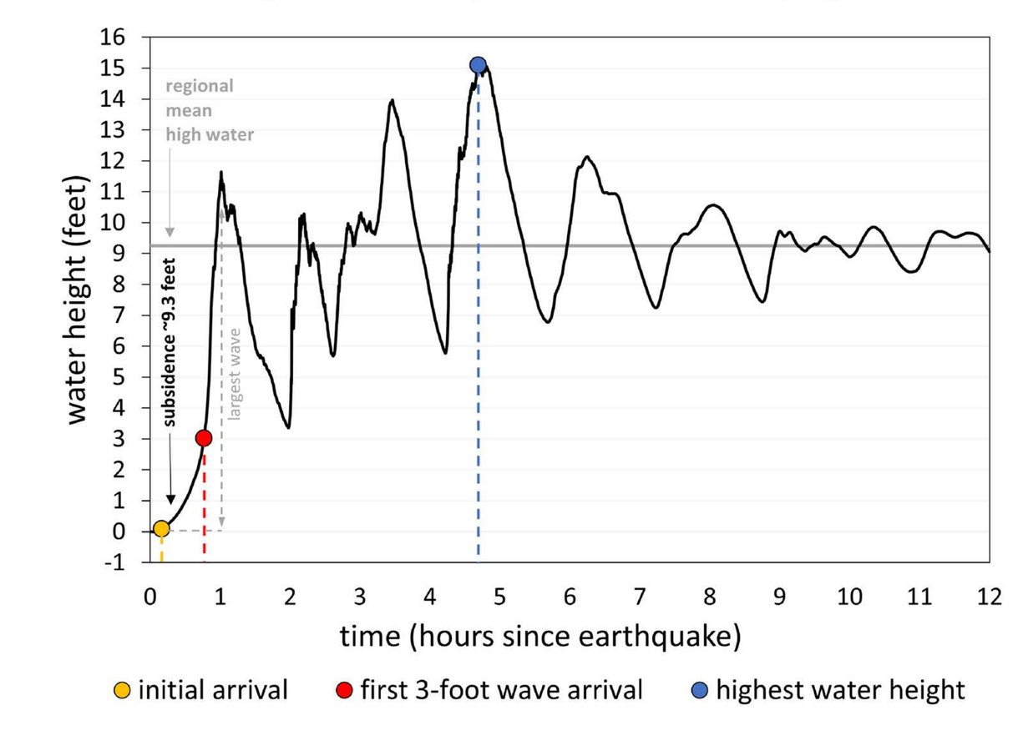

Figure 6. Wishkah simulated tide gauge

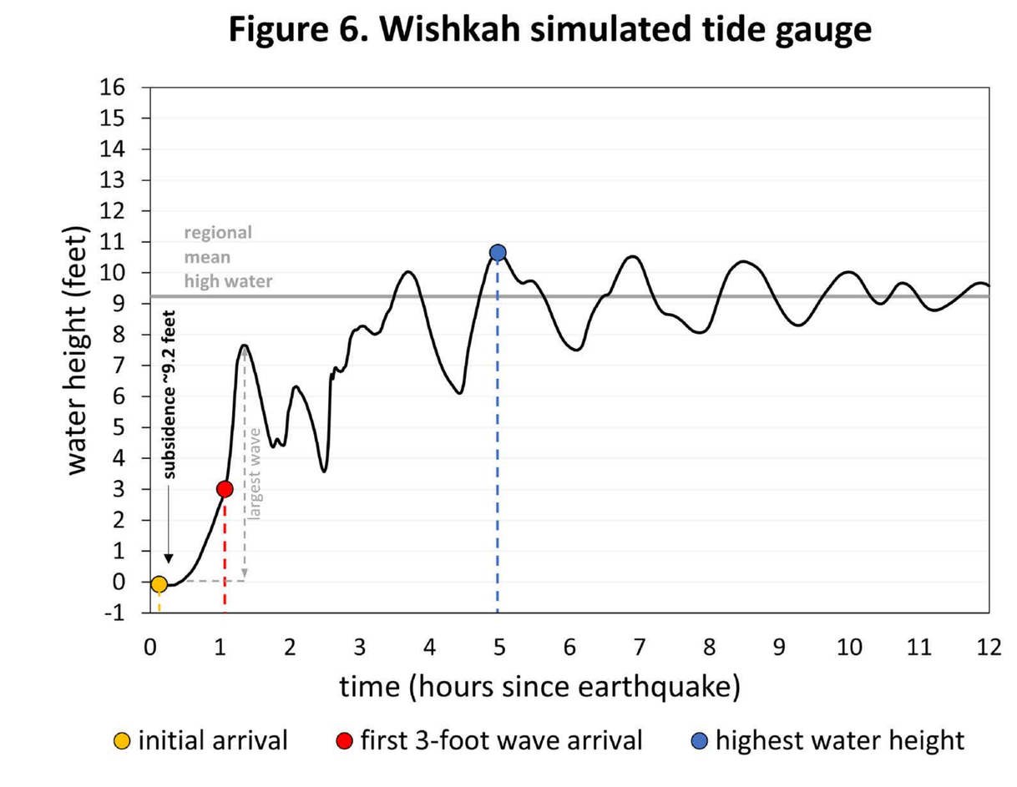

Figures 3–6. Modeled tsunami wave variations over 12 hours of simulated time at the mouths of the Chehalis (Fig. 3), Hoquiam (Fig. 4), Willapa (Fig. 5), and Wishkah (Fig. 6) Rivers. Coseismic subsidence causes the land and sea surface elevation to drop from the mean high water model datum simultaneously. Thus, there is no change in water height right after the earthquake, relative to an observer on land. Although the first modeled wave often represents the largest change in water height, the highest overall water height occurs much later. This height includes both tsunami inundation from the earthquake-generated wave and the amount of sea-surface recovery following subsidence. This recovery represents the subsided sea surface level eventually rebounding back to pre-subsidence conditions during the simulation time.

Upriver Flooding Extent

Upriver flooding impacts are greatest within the Willapa River (Map 3). Here, overall inundation travels as far as 12 river miles (19.3 kilometers) upriver from the Willapa Harbor Airport to the town of Willapa. For the first time, this modeling identifies the city of Raymond as being located within the tsunami inundation zone. Here, the tsunami floods nearly the entire city, with average inundation depths between 5–8 feet (1.5–2.4 meters), except for the high-ground "island" on the eastern city limit (Map 3). The tsunami also travels extensively up the Chehalis, Hoquiam, and Wishkah Rivers. For instance, the tsunami inundates approximately 8 river miles (12.9 kilometers) up both the Hoquiam (west and east forks) and Wishkah Rivers (Map 1). On the west fork of the Hoquiam, multiple sections of US-101 are inundated with 4–8 feet (1.3–2.4 meters) of flooding. This presumably isolates the communities to the north, such as New London. Similarly, along the Wishkah River, the modeled tsunami inundation may isolate the Aberdeen Gardens community as well with similar flooding depths. Tsunami inundation travels the farthest up the Chehalis River, flooding the low-lying areas of the river valley and reaching the area just east of Montesano near Schafer Boom Road approximately 13 river miles (21 kilometers) from the US-101 Bridge. Sections of the Puget Sound and Pacific railroad grade sit within the modeled inundation zone near Central Park and could face flooding depths as deep as 8 feet (2.4 meters).

Current Speed

Map 4 shows four ranges of tsunami current speeds in knots (a knot is equal to 1 nautical mile/hr or ~1.15 land mi/hr): 0–3 knots, 3–6 knots, 6–9 knots, and >9 knots. These binned ranges follow the port damage categorization of Lynett and others (2014). The ranges approximate hazard to ships and docking facilities representing: no expected damage (0–3 knots), minor/moderate damage possible (3–6 knots), major damage possible (6–9 knots), and extreme damage possible (>9 knots).

In general, modeled current speeds tend to decrease farther upriver and away from Grays Harbor and Willapa Bay. The fastest current speeds in the newly modeled areas within the Hoquiam and Wishkah Rivers are less than 3 knots, falling into the lowest damage categorization. In the Chehalis River, only the westernmost edge of the new model data shows current speeds in the 3–6 knot range, where minor to moderate damage is possible. However, in the stretch of the Willapa River downstream of Raymond, small areas of currents in the 6–9 knot range were captured in the tsunami simulation. The tsunami may entrain debris from infrastructure downstream.

LIMITATIONS OF THE MODEL

The rupture patterns of earthquakes on a given subduction zone often vary significantly from one earthquake sequence to the next. In addition, because there have been no direct observations of previous coseismic slip produced in a large CSZ earthquake, there is substantial uncertainty in the resultant pattern of seafloor deformation (uplift and subsidence) in the next event. The L1 scenario used in this study is deterministic and has a simplified regional slip distribution along a splay fault that only takes into account the static, vertical component of seafloor displacement for tsunami generation (Witter and others, 2011). This scenario ruptures instantaneously in our modeling along the CSZ margin and does not include other potential components that could alter the tsunami generation, such as material heterogeneity in the subduction zone (see the University of Washington M9 project; https://hazards.uw.edu/geology/m9/), inelastic behavior, horizontal slip components, extensional faults within the subduction zone, induced submarine landslides, or dynamic coseismic deformation. The next earthquake may have a more complex slip distribution and rupturing geometry than the modeled scenario.

The tsunami modeling presented here was simulated using the MHW vertical reference datum and does not include the influences of changes in tides. The diurnal range (the difference in height between mean higher high water and mean lower low water) is 9.14 ft (2.79 m) at Westport, Washington (NOAA, 2020) and overall tsunami inundation is tied to the tide stage. The results included in this study are conservative when compared to tsunami models that use a lower static tide stage. Modeled upriver tsunami propagation does not include natural riverine flow either. Both interactions with tidal currents and riverine flow can be additive if in the same direction or steepen the tsunami wave front, causing a breaking wave if in an opposing direction (Zhang and others, 2011). Additionally, the GeoClaw software has limitations when simulating interactions between an ebbing wave and a subsequent flooding wave.

Furthermore, this modeling incorporates high-resolution elevation data from a bare-earth DEM, meaning that it does not include engineered structures, buildings, or trees. Not including these features leads our models to generally produce greater inundation and a more conservative model result compared to if they were included. However, simulating a model that assumes bare-earth topography may neglect possible localized effects that vegetation and structures can have on the path and flow of the tsunami. For example, higher fluid velocities, greater turbulence, and different trajectories may exist in regions where a neighboring building or vegetation could channelize flow. This may lead to locally faster current speeds in actuality. A more realistic assessment of tsunami impacts would require additional site-specific modeling using an all-returns topographic model (incorporating buildings, vegetation, and infrastructure).

These model results do not account for the possibility of seismically induced seiches or tsunamigenic landslides resulting from the earthquake. Seiches are a series of standing waves that may occur in fully or partially enclosed bodies of water when earthquake waves pass through. Additionally, the modeling does not include any foreshocks or aftershocks, which may also cause slope failures that could generate tsunamis. The contributions of projected sea-level rise to tsunami inundation were also not explored in this study.

Despite some limitations to our model, meaning that the model does not provide an exact representation of a tsunami generated by an earthquake on the Cascadia subduction zone, the results presented here are valuable for regional awareness and hazard planning. We emphasize that planning for tsunami hazards also includes planning for earthquake hazards. We hope this information will be used to increase community resilience to tsunamis and earthquakes in the communities of southwest Washington.

ACKNOWLEDGMENTS

We acknowledge the previous tsunami modeling within Grays Harbor and Willapa Bay completed by NOAA PMEL, which provided a basis for the new modeling presented in this publication. Additionally, we thank the WGS Publications Group for their efforts in editing and producing the tsunami inundation and current speed map figures, specifically Daniel Coe. We also would like to acknowledge Guy McWethy, Lidar Specialist with the WGS Lidar Program, for incorporating new lidar data into the existing DEM used in tsunami modeling. This modeling would not be possible without the seminal work of Witter and others (2011), who developed the Cascadia subduction zone earthquake source model.

REFERENCES

Atwater, B. F., 1988, Geologic studies for seismic zonation of the Puget Lowland. *In* Jacobson, M. L.; Rodriguez, T. R., compilers, National Earthquake Hazards Reduction Program, Summaries of technical reports, Volume XXV: U.S. Geological Survey Open-File Report 88-16, p. 120–133. [https://doi.org/10.3133/ofr8816]

Atwater, B. F., 1992, Geologic evidence for earthquakes during the past 2000 years along the Copalis River, southern coastal Washington: Journal of Geophysical Research, v. 97, no. B2, p. 1901–1919. [https://doi.org/10.1029/91JB02346]

Atwater, B. F.; Hemphill-Haley, Eileen, 1997, Recurrence intervals for great earthquakes of the past 3,500 years at northeastern Willapa Bay, Washington: U.S. Geological Survey Professional Paper 1576, 108 p. [https://doi.org/10.3133/pp1576]

Atwater, B. F.; Nelson, A. R.; Clague, J. J.; Carver, G. A.; Yamaguchi, D. K.; Bobrowsky, P. T.; Bourgeois, Joanne; Darienzo, M. E.; Grant, W. C.; Hemphill-Haley, Eileen; Kelsey, H. M.; Jacoby, G. C.; Nishenko, S. P.; Palmer, S. P.; Peterson, C. D.; Reinhart, M. A., 1995, Summary of coastal geologic evidence for past great earthquakes at the Cascadia subduction zone: Earthquake Spectra, v. 11, no. 1, 18 p. [https://doi.org/10.1193/1.1585800]

Berger, M. J.; George, D. L.; LeVeque, R. J.; Mandli, K. T., 2011, The GeoClaw software for depth-averaged flows with adaptive refinement: Advances in Water Resources, v. 34, no. 9, p. 1195–1206. [https://doi.org/10.1016/j.advwatres.2011.02.016]

Clawpack Development Team, 2023, Clawpack Version 5.9.0. [http://www.clawpack.org]

Dolcimascolo, Alexander; Eungard, D. W.; Allen, Corina; LeVeque, R. J.; Adams, L. M.; Arcas, Diego; Titov, V. V.; González, F. I.; Moore, Christopher; Garrison-Laney, C. E.; Walsh, T. J., 2021, Tsunami hazard maps of the Puget Sound and adjacent waters—Model results from an extended L1 Mw 9.0 Cascadia subduction zone megathrust earthquake scenario: Washington Geological Survey Map Series 2021-01, originally published 2021, 16 sheets, scale 1:48,000, 49 p. text. [https://fortress.wa.gov/dnr/geologydata/tsunami_hazard_-maps/ger_ms2021-01_tsunami_haz- ard_puget_sound.zip]

Eungard, D. W.; Forson, Corina; Walsh, T. J.; Gica, Edison; Arcas, Diego, 2018, Tsunami hazard maps of southwest Washington—Model results from a ~2,500-year Cascadia subduction zone earthquake scenario [Revised May 2018]: Washington Geological Survey Map Series 2018-01, originally published March 2018, 6 sheets, scale 1:48,000, 11 p. text. [https://www.dnr.wa.gov/publications/ger_ms2018-01_tsunami_hazard_southwest_washington.zip]

George, D. L., 2006, Finite volume methods and adaptive refinement for tsunami propagation and inundation: University of Washington Doctor of Philosophy thesis, 167 p. [https://digital.lib.washington.edu/researchworks/handle/1773/4639]

George, D. L., 2008, Augmented Riemann solvers for the shallow water equations over variable topography with steady states and inundation: Journal of Computational Physics, v. 227, no. 6, p. 3089–3113. [https://doi.org/10.1016/j.jcp.2007.10.027]

George, D. L.; LeVeque, R. J., 2006, Finite volume methods and adaptive refinement for global tsunami propagation and local inundation: Science of Tsunami Hazards, v. 24, no. 5, p. 319–328. [https://digital.lib.washington.edu/researchworks/bitstream/handle/1773/4639/tsunami06.pdf]

González, F. I.; LeVeque, R. J.; Chamberlain, Paul; Hirai, Bryant; Varkovitsky, Jonathan; George, D. L., 2011, Validation of the GeoClaw model—NTHMP MMS tsunami inundation model validation workshop: University of Washington, 84 p. [https:// depts.washington.edu/clawpack/links/nthmp-benchmarks/geoclaw-results.pdf]

Goldfinger, Chris; Nelson, C. H.; Morey, A. E.; Johnson, J. E.; Patton, J. R.; Karabanov, Eugene; Gutierrez-Pastor, Julia; Eriksson, A. T.; Gracia, Eulalia; Dunhill, Gita; Enkin, R. J.; Dallimore, Audrey; Vallier, Tracy, 2012, Turbidite event history—Methods and implications for Holocene paleoseismicity of the Cascadia subduction zone: U.S. Geological Survey Professional Paper 1661-F, 170 p. [https://pubs.usgs.gov/pp/pp1661f/]

Horrillo, Juan; Grilli, S. T.; Nicolsky, Dmitry; Roeber, Volker; Zhang, Joseph, 2015, Performance benchmarking tsunami models for NTHMP's inundation mapping activities: Pure and Applied Geophysics, v. 172, no. 3–4, p. 869–884. [https://doi.org/10.1007/s00024-014-0891-y]

Hutchinson, Ian; Clague, John, 2017, Were they all giants? Perspectives on late Holocene plate-boundary earthquakes at the northern end of the Cascadia subduction zone: Quaternary Science Reviews, v. 169, p. 29–49. [https://doi.org/10.1016/j.quascirev.2017.05.015]

Kelsey, H. M.; Nelson, A. R.; Hemphill-Haley, Eileen; Witter, R. C., 2005, Tsunami history of an Oregon coastal lake reveals a 4600 yr record of great earthquakes on the Cascadia subduction zone: Geological Society of America Bulletin, v. 117, no. 7–8, p. 1009–1032. [https://doi.org/10.1130/B25452.1]

Leonard, L. J.; Currie, C. A.; Mazzotti, Stéphane; Hyndman, R. D., 2010, Rupture area and displacement of past Cascadia great earthquakes from coastal coseismic subsidence: Geological Society of America Bulletin, v. 122, no. 11–12, p. 2079–2096. [https://doi.org/10.1130/B30108.1]

LeVeque, R. J.; George, D. L.; Berger, M. J, 2011, Tsunami modelling with adaptively refined finite volume methods: Acta Numerica, v. 20, p. 211–289. [https://doi.org/10.1017/S0962492911000043]

Lynett, P. J.; Borrero, Jose; Son, Sangyoung; Wilson, Rick; Miller, Kevin, 2014, Assessment of the tsunami-induced current hazard: Geophysical Research Letters, v. 41, no. 6, p. 2048–2055. [https://doi.org/10.1002/2013GL058680]

Mandli, K. T.; Ahmadia, A. J.; Berger, Marsha; Calhoun, Donna; George, D. L.; Hadjimichael, Yiannis; Ketcheson, D. I.; Lemoine, G. I.; LeVeque, R. J., 2016, Clawpack: Building an open source ecosystem for solving hyperbolic PDEs: PeerJ Computer Science, v. 2, no. e68, 27 p. [https://doi.org/10.7717/peerj-cs.68]

NOAA National Geophysical Data Center (NGDC), 2012, Astoria, Oregon 1/3 Arc-second MHW Coastal Digital Elevation Model: NOAA National Centers for Environmental Information, [accessed Jul. 17, 2023 at https://www.ncei.noaa.gov/metadata/geoportal/rest/metadata/item/gov.noaa.ngdc.mgg.dem:5490/html].

NOAA, 2020, Tides and Currents: Datums for 9441102, Westport WA [website], National Oceanic and Atmospheric Administration. [accessed August 31, 2023 at https://tidesandcurrents.noaa.gov/datums.html?id=9441102]

NOAA, 2023, NOAA Electronic Navigational Charts (ENC). [https://www.fisheries.noaa.gov/inport/item/39976]

Padgett, J. S.; Engelhart, S. E.; Kelsey, H. M.; Witter, R. C.; Cahill, Niamh; Hemphill-Haley, Eileen, 2021, Timing and amount of southern Cascadia earthquake subsidence over the past 1700 years at northern Humboldt Bay, California, USA: Geological Society of America Bulletin, v. 133, no. 9–10, p. 2137–2156. [https://doi.org/10.1130/B35701.1]

Synolakis, C. E.; Bernard, E. N.; Titov, V. V.; Kânoğlu, Utku; González, F. I., 2007, Standards, criteria, and procedures for NOAA evaluation of tsunami numerical models: National Oceanic and Atmospheric Administration Technical Memorandum OAR PMEL-135, 60 p. [https://repository.library.noaa.gov/view/noaa/11073/-noaa_11073_DS1.pdf]

Titov, V. V.; Arcas, Diego; Moore, C. W.; LeVeque, R. J.; Adams, L. M.; González, F. I., 2018, Tsunami hazard assessment of Bainbridge Island, Washington Project Report: Washington State Emergency Management Division, 43 p. [http://depts.washington.edu/ptha/WA_EMD_Bainbridge/BainbridgeIslandTHA.pdf]

USGS, 2019a, Olympics South Opsw 2019, Olympic Peninsula Area 1 LiDAR Project, collected between Sept. 14th, 2017 and Apr. 25, 2019 by Quantum Spatial Inc., 3-ft resolution, accessed Apr. 12, 2023 [http://lidarportal.dnr.wa.gov/], metadata available on portal [ger_olympics_south_opsw_2019_lidar_report.pdf]

USGS, 2019b, Southwest WA Opsw 2019, Olympic Peninsula Area 2 LiDAR Project, collected between Feb. 19, 2018 and Apr. 25, 2019 by Quantum Spatial Inc., 3-ft resolution, accessed Apr. 12, 2023 [http://lidarportal.dnr.wa.gov/], metadata available on portal [ger_southwest_wa_opsw_2019_lidar_report.pdf]

Witter, R. C.; Zhang, Y. J.; Wang, Kelin; Priest, G. R.; Goldfinger, Chris; Stimely, L. L.; English, J. T.; Ferro, P. A., 2011, Simulating tsunami inundation at Bandon, Coos County, Oregon, using hypothetical Cascadia and Alaska earthquake scenarios: Oregon Department of Geology and Mineral Industries Special Paper 43, 57 p. [http://www.oregongeology.org/pubs/sp/p-SP-43.htm]

Zhang, Y. J.; Witter, R. C.; Priest, G. R., 2011, Tsunami-tide interaction in 1964 Prince William Sound tsunami: Ocean Modelling, v. 40, no. 3–4, p. 246–259. [https://doi.org/10.1016/j.ocemod.2011.09.005]

WASHINGTON GEOLOGICAL SURVEY
MAP SERIES 2023-02

Tsunami Hazard Maps of the Chehalis, Hoquiam, Willapa, and Wishkah Rivers—Model Results from a L1 Mw 9.0 Cascadia Subduction Zone Megathrust Earthquake Scenario
December 2023

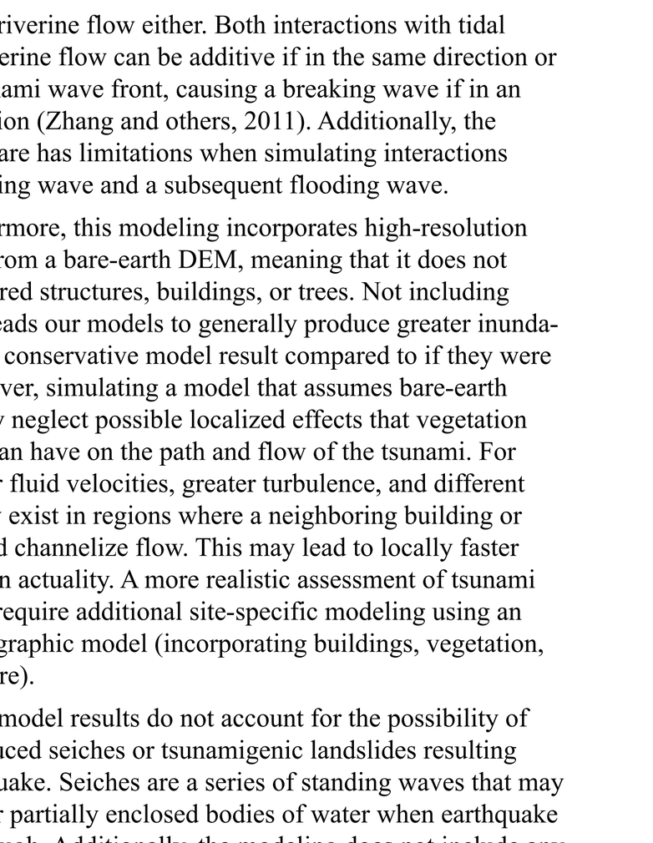

Shaded relief generated from a composite lidar 3-foot horizontal-resolution digital elevation model, HARN State Plane coordinate system, Washington South FIPS 4602 North American Datum of 1983

Road data: © OpenStreetMap contributors, openstreetmap.org

Digital cartography by Daniel E. Coe

Editing and production by Susan R. Schnur and Daniel E. Coe

Suggested citation: Dolcimascolo, Alexander; Eungard D. W.; Allen, Corina, 2023, Tsunami hazard maps of the Chehalis, Hoquiam, Willapa, and Wishkah Rivers—Model results from an L1 Mw 9.0 Cascadia subduction zone megathrust earthquake scenario: Washington Geological Survey Map Series 2023-02, 1 sheet, scale 1:48,000 and 1:166,000. [https://fortress.wa.gov/dnr/geologydata/tsunami_hazard_maps/ger_ms2023-02_tsunami_hazard_sw_wa_rivers.pdf]

MAP SCALE 1:166,000
10 miles

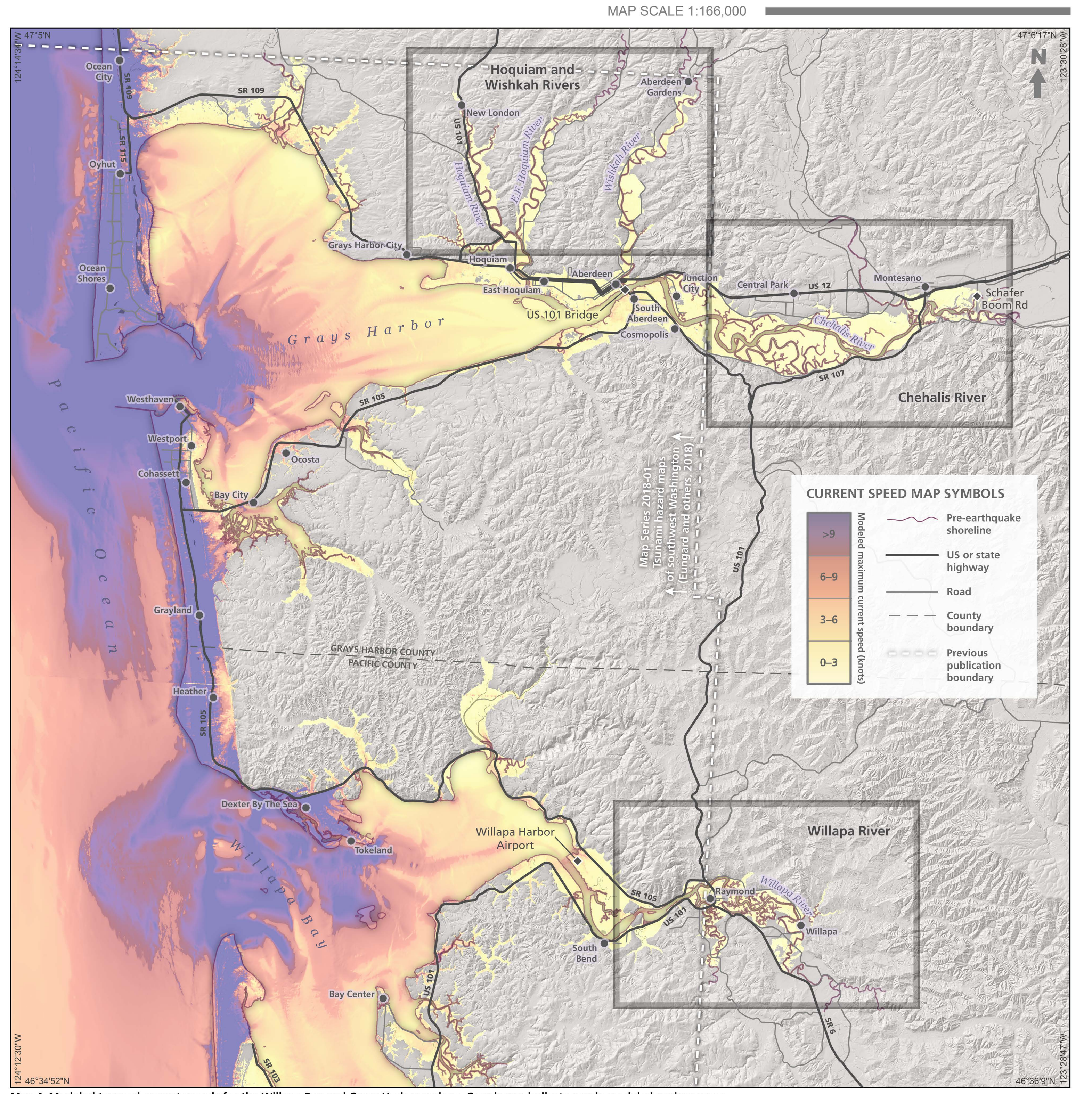

Map 4. Modeled tsunami current speeds for the Willapa Bay and Grays Harbor regions. Gray boxes indicate newly modeled upriver areas.